Rectifier Design for Minimum Line-Current Harmonics and Maximum Power Factor

Arthur W. Kelley, *Member, IEEE,* and William F. Yadusky, *Member, IEEE*

Abstract—**Rectifier line-current harmonics interfere with proper power system operation, reduce rectifier power factor, and limit the power available from a given service. The rectifier's output filter inductance determines the rectifier line-current waveform, the line-current harmonics, and the power factor. Classical rectifier analysis usually assumes a near-infinite output filter inductance, which introduces significant error in the estimation of line-current harmonics and power factor. This paper presents a quantitative analysis of single- and three-phase rectifier line-current harmonics and power factor as a function of the output filter inductance. For the single-phase rectifier, one value of finite output filter inductance produces maximum power factor and a different value of finite output filter inductance produces minimum line-current harmonics. For the three-phase rectifier, a near-infinite output filter inductance produces minimum line-current harmonics and maximum power factor, and the smallest inductance that approximates a near-infinite inductance is determined.**

I. Introduction

HIGH line-current harmonics and low power factor have recently received increased scrutiny from both power-systems and power-electronics perspectives due to increased installation of rectifiers in applications such as machine drives, electronic lighting ballasts, and uninterruptible power supplies. Line-current harmonics prevent full utilization of the installed service by increasing the rms line current without delivering power and reduce rectifier power factor. Line-current harmonics cause overheating of power system components, and trigger protective devices prematurely. In addition, propagation of line-current harmonics into the power system interferes with the operation of sensitive electronic equipment sharing the rectifier supply.

Full-wave rectifiers, as shown in Fig. 1 convert a single-phase ac source v_S or a three-phase ac source v_{SA}, v_{SB}, and v_{SC} to a high-ripple dc voltage v_X. The output filter, consisting of L_O and C_O, attenuates the ripple in v_X and supplies a low-ripple unregulated dc voltage V_O to the load. In a simplified analysis, v_S is a zero-impedance source, and v_{SA}, v_{SB}, and v_{SC} are balanced zero-impedance sources. The diodes are piecewise-linear elements modeled as ideal switches with zero-forward voltage drop when on, zero reverse leakage current when off, and instantaneous switching. The output filter inductor L_O and capacitor C_O are linear and lossless. A near-infinite output capacitor C_O and a near-zero-ripple capacitor voltage v_{CO} are also assumed. Using these assumptions, the output filter inductance L_O determines the rectifier line-current harmonics and power factor, but this important relationship is frequently subverted by the further assumption of a near-infinite L_O resulting in a near-zero-ripple inductor current i_X. Overly simplified waveshapes for single-phase rectifier line current i_S and three-phase rectifier line currents i_{SA}, i_{SB}, and i_{SC} result, and grossly inaccurate estimates of rectifier line-current harmonics and power factor are produced.

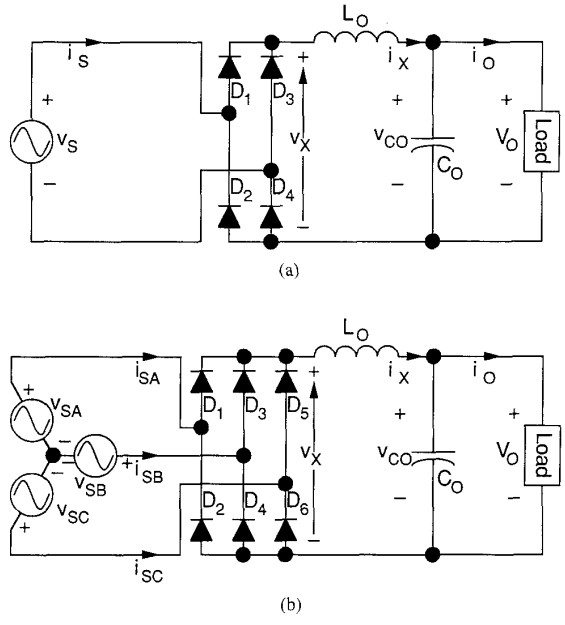

Fig. 1. Rectifiers commonly used for conversion of power system ac voltage to unregulated dc. (a) Single-phase rectifier. (b) Three-phase rectifier.

Manuscript received November 28, 1989; revised August 1, 1991. This research was sponsored by the Electric Power Research Center of North Carolina State University and supported by the National Science Foundation under grant ECS-8806171. The original version of this paper was presented at the 1989 Applied Power Electronics Conference (APEC'89), Baltimore, MD, March 13–17, 1989.

A. W. Kelley is with the Department of Electrical and Computer Engineering, North Carolina State University, Raleigh, NC 27695-7911.

W. F. Yadusky was with North Carolina State University when this work was performed and is now with Exide Electronics, 3201 Spring Forest Road, Raleigh, NC 27604.

IEEE Log Number 9106960.

tor that is verified by comparison with laboratory measurement and presents design curves for rectifier line-current harmonics and power factor as a function of a output filter inductance L_O. For the single-phase rectifier, the classical near-infinite output filter inductor is shown to produce maximum power factor, but not to produce minimum rectifier line-current harmonics, and the inductance that produces minimum rectifier line-current harmonics is determined. For the three-phase rectifier, a near-infinite output filter inductor is shown to produce minimum rectifier line-current harmonics and maximum power factor, and the minimum value of output inductance needed to approximate an infinite inductor is determined.

II. Normalization

Before the rectifier analysis and design relationships are developed, the rectifiers of Fig. 1 are normalized with respect to the set of references shown in Table I to produce the normalized rectifiers shown in Fig. 2. Note that an $-N$ appended to a subscript indicates a normalized quantity. However, angles in either degrees or radians are already normalized with respect to the period of the fundamental of source voltage, have the same numerical value in both the normalized and circuit domains, and the $-N$ is omitted from the subscript for angles.

Normalization is based on three principal references: a voltage reference, a power reference, and a frequency (or time) reference. For the single-phase rectifier, the nominal rms value $V_{S(\text{nom})}$ of the source voltage v_S is the voltage reference V_{REF}. For the three-phase rectifier, the nominal rms value $V_{SA(\text{nom})} = V_{SB(\text{nom})} = V_{SC(\text{nom})}$ of the balanced line-to-neutral source voltage is the voltage reference. The nominal rectifier output power $P_{O(\text{nom})}$ is the power reference P_{REF}. The nominal source frequency $f_{S(\text{nom})}$ is the frequency reference f_{REF}, where the nominal period of the source $T_{S(\text{nom})} = 1/f_{S(\text{nom})}$ is the companion time reference $T_{\text{REF}} = 1/f_{\text{REF}}$.

The voltage and power references are used to derive a current reference $I_{\text{REF}} = P_{\text{REF}}/V_{\text{REF}}$, which is the rms current drawn from a voltage source V_{REF} by a linear load of apparent power equal in magnitude to P_{REF}. Similarly, the impedance reference $Z_{\text{REF}} = V_{\text{REF}}/I_{\text{REF}} = V_{\text{REF}}^2/P_{\text{REF}}$ is the impedance of a linear load connected to V_{REF} drawing apparent power P_{REF}.

Table II shows the normalization and design relationships based on the references of Table I. The normalization relationships, (N.1)–(N.13), translate rectifier circuit quantities into dimensionless normalized quantities for comparison with the normalized design curves found in this paper. For example, as shown by (N.4) the normalized single-phase source voltage $v_{S\text{-}N}$ is the dimensionless ratio of the actual source voltage v_S to the voltage reference V_{REF}; as shown by (N.5) the normalized single-phase rectifier current $i_{S\text{-}N}$ is the ratio of the actual rectifier current i_S to the current reference I_{REF}. The normalized value of a circuit element is found from the normalized impedance of that element at frequency f_{REF}. For example, the normalized impedance $Z_{LO\text{-}N}$ of the output filter inductor

TABLE I
Normalization References

Quantity	Symbol	Value
Voltage	V_{REF}	$= V_{S(\text{nom})}$—(single-phase rectifier) nominal rms source voltage $= V_{SA(\text{nom})} = V_{SB(\text{nom})} = V_{SC(\text{nom})}$—(three-phase rectifier) nominal rms line-to-neutral source voltage
Power	P_{REF}	$= P_{O(\text{nom})}$—nominal rectifier output power
Frequency	f_{REF}	$= f_{S(\text{nom})}$—nominal frequency of source
Time	T_{REF}	$= T_{S(\text{nom})} = 1/f_{S(\text{nom})}$—nominal period of source
Current (derived)	I_{REF}	$= P_{\text{REF}}/V_{\text{REF}}$—rms current drawn from voltage reference V_{REF} by linear load of apparent power P_{REF}
Impedance (derived)	Z_{REF}	$= V_{\text{REF}}^2/P_{\text{REF}}$—impedance of linear load drawing apparent power P_{REF} from source V_{REF}

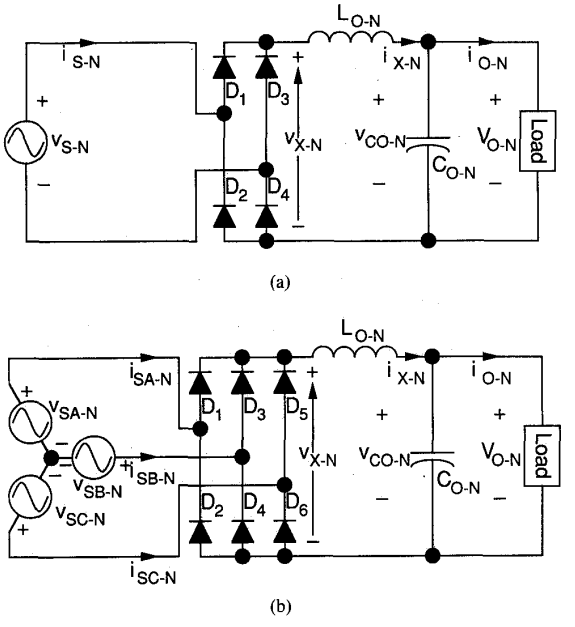

Fig. 2. Rectifiers of Fig. 1 normalized with respect to voltage, power, and frequency references of Table I. (a) Normalized single-phase rectifier. (b) Normalized three-phase rectifier.

L_O is the ratio of the inductor impedance Z_{LO} at the reference frequency to the reference impedance Z_{REF}:

$$Z_{LO\text{-}N} = \frac{Z_{LO}}{Z_{\text{REF}}} = \frac{(2\pi f_{\text{REF}})L_O}{V_{\text{REF}}/I_{\text{REF}}}$$

$$= 2\pi \frac{I_{\text{REF}} f_{\text{REF}}}{V_{\text{REF}}} L_O = 2\pi L_{O\text{-}N} \qquad (1)$$

TABLE II
NORMALIZATION AND DESIGN RELATIONSHIPS

Normalization Relationships	Eqn. No.	Design Relationships	Eqn. No.
$t_N = t/T_{REF}$	N.1	$t = t_N T_{REF}$	D.1
$T_{S\text{-}N} = T_S/T_{REF}$	N.2	$T_S = T_{S\text{-}N} T_{REF}$	D.2
$f_{S\text{-}N} = f_S/f_{REF}$	N.3	$f_S = f_{S\text{-}N} f_{REF}$	D.3
$v_{S\text{-}N} = v_S/V_{REF}$ $v_{SA\text{-}N} = v_{SA}/V_{REF}$ $v_{SB\text{-}N} = v_{SB}/V_{REF}$ $v_{SC\text{-}N} = v_{SC}/V_{REF}$	N.4	$v_S = v_{S\text{-}N} V_{REF}$ $v_{SA} = v_{SA\text{-}N} V_{REF}$ $v_{SB} = v_{SB\text{-}N} V_{REF}$ $v_{SC} = v_{SC\text{-}N} V_{REF}$	D.4
$i_{S\text{-}N} = i_S/I_{REF}$ $i_{SA\text{-}N} = i_{SA}/I_{REF}$ $i_{SB\text{-}N} = i_{SB}/I_{REF}$ $i_{SC\text{-}N} = i_{SC}/I_{REF}$	N.5	$i_S = i_{S\text{-}N} I_{REF}$ $i_{SA} = i_{SA\text{-}N} I_{REF}$ $i_{SB} = i_{SB\text{-}N} I_{REF}$ $i_{SC} = i_{SC\text{-}N} I_{REF}$	D.5
$v_{X\text{-}N} = v_X/V_{REF}$	N.6	$v_X = v_{X\text{-}N} V_{REF}$	D.6
$i_{X\text{-}N} = i_X/I_{REF}$	N.7	$i_X = i_{X\text{-}N} I_{REF}$	D.7
$i_{O\text{-}N} = i_O/I_{REF}$	N.8	$i_O = i_{O\text{-}N} I_{REF}$	D.8
$v_{CO\text{-}N} = v_{CO}/V_{REF}$	N.9	$v_{CO} = v_{CO\text{-}N} V_{REF}$	D.9
$V_{O\text{-}N} = V_O/V_{REF}$	N.10	$V_O = V_{O\text{-}N} V_{REF}$	D.10
$P_{O\text{-}N} = P_O/P_{REF}$	N.11	$P_O = P_{O\text{-}N} P_{REF}$	D.11
$L_{O\text{-}N} = L_O(I_{REF} f_{REF}/V_{REF})$	N.12	$L_O = L_{O\text{-}N}(V_{REF}/I_{REF} f_{REF})$	D.12
$C_{O\text{-}N} = C_O(V_{REF} f_{REF}/I_{REF})$	N.13	$C_O = C_{O\text{-}N}(I_{REF}/V_{REF} f_{REF})$	D.13

and the normalized output filter inductance $L_{O\text{-}N}$ is defined by (N.12).

The design relationships, (D.1)–(D.13) of Table II, are simply the inverse of the normalization relationships and translate dimensionless normalized quantities into actual circuit quantities. Rectifier design for minimum line-current harmonics and maximum power factor uses the design relationships to choose actual circuit quantities based on desired normalized quantities. Examples of single- and three-phase rectifier design are presented subsequently.

III. Classical Analysis

Traditionally, the principal output-filter design criterion is attenuation of output voltage ripple, and the relationship between output filter design and rectifier line-current harmonics and power factor is ignored. The classical line-current analysis assumes a near-infinite output filter capacitance $C_{O\text{-}N}$ causing a near-zero-ripple output filter capacitor voltage $v_{CO\text{-}N}$, and also assumes a near-infinite output filter inductance $L_{O\text{-}N}$ causing a near-zero-ripple output filter inductor current $i_{X\text{-}N}$ [1]. The single- and three-phase rectifier waveforms that result from these assumptions are shown in Fig. 3. The rectifier line-current waveforms are easily analyzed for line-current harmonics and power factor, which explains the popularity of the classical analysis.

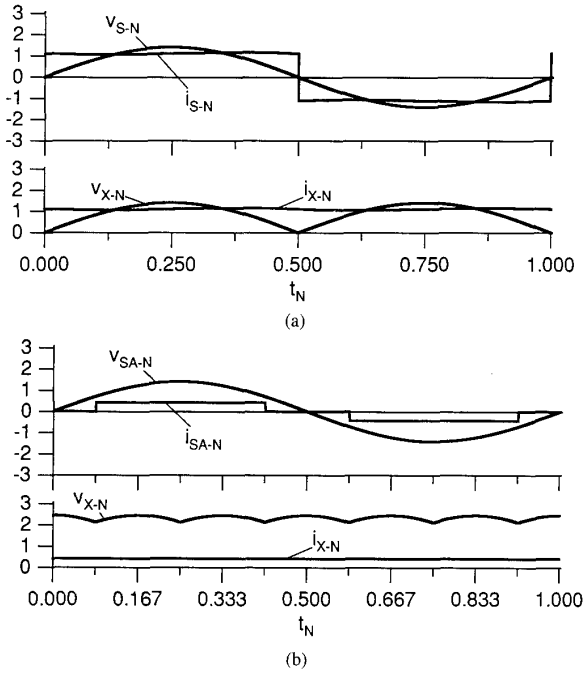

Fig. 3. Normalized rectifier waveforms for near-infinite output filter inductance and near-zero-ripple output filter inductor current. (a) Single-phase rectifier source voltage $v_{S\text{-}N}$, rectifier line current $i_{S\text{-}N}$, rectifier output voltage $v_{X\text{-}N}$, and output filter inductor current $i_{X\text{-}N}$. (b) Three-phase rectifier phase-A source voltage $v_{SA\text{-}N}$, phase-A rectifier line current $i_{SA\text{-}N}$, rectifier output voltage $v_{X\text{-}N}$, and output filter inductor current $i_{X\text{-}N}$.

In practice, the output filter capacitor $C_{O\text{-}N}$ *is usually* large enough to produce sufficiently near-zero-ripple output filter capacitor voltage $v_{O\text{-}N}$ with respect to rectifier line-current harmonics and power factor, and this assumption is often justified. However, the assumption of near-infinite output filter inductance and near-zero-ripple output filter inductor current $i_{X\text{-}N}$ *is almost never* met in practice and produces gross errors in the classical analysis of rectifier line-current harmonics and power factor. Practical rectifier line-current waveshapes are much more complex than those shown in Fig. 3, and the following section describes a computer simulation for determining these waveshapes.

IV. Computer Simulation

The normalized rectifier waveforms in the periodic steady-state condition are determined by time-domain computer simulation. Subsequent analysis of the waveforms determines the line-current harmonics and power factor. The time-domain simulation of circuits is a well-developed analysis technique, and has been often described in the literature [2], [3]. The simulation techniques used to produce the results reported in this paper are summarized in this section.

The nonlinear differential equations that describe both single- and three-phase rectifiers are cast in the same state-variable formulation. The two state variables are the output filter inductor current $i_{X\text{-}N}$ and the output filter capac-

itor voltage $v_{CO\text{-}N}$. The state equations for both rectifiers are:

$$\frac{dv_{CO\text{-}N}}{dt_N} = \frac{1}{C_{O\text{-}N}}[i_{X\text{-}N} - i_{O\text{-}N}] = \frac{1}{C_{O\text{-}N}}\left(i_{X\text{-}N} - \frac{P_{O\text{-}N}}{v_{CO\text{-}N}}\right) \quad (2)$$

$$\frac{di_{X\text{-}N}}{dt_N} = \frac{1}{L_{O\text{-}N}}(v_{X\text{-}N} - v_{CO\text{-}N}). \quad (3)$$

The values of $L_{O\text{-}N}$ and $C_{O\text{-}N}$ are constant. In addition, a constant output power load is assumed and $P_{O\text{-}N}$ is held constant. Therefore, (2) is nonlinear due to the reciprocal relationship of output current $i_{O\text{-}N}$ and capacitor voltage $v_{CO\text{-}N}$ for constant output power $P_{O\text{-}N}$.

For the single-phase rectifier, the nonlinearity of diodes D_1–D_4 is embedded in (3) because the filter input voltage $v_{X\text{-}N}$ is a function of the diodes' state as determined by the voltage source $v_{S\text{-}N}$, and the state variables $i_{X\text{-}N}$ and $v_{CO\text{-}N}$. If $i_{X\text{-}N} > 0$ or $|v_{S\text{-}N}| > v_{CO\text{-}N}$, then one pair of diodes is on with $v_{X\text{-}N} = |v_{S\text{-}N}|$, and $i_{X\text{-}N}$ circulates through the voltage source. If $i_{X\text{-}N} = 0$ and $|v_{S\text{-}N}| < v_{CO\text{-}N}$, then all diodes are off, $v_{X\text{-}N} = v_{CO\text{-}N}$, and the current through the voltage source is zero.

Similarly for the three-phase rectifier, the nonlinearity of diodes D_1–D_6 is embedded in (3) because the filter input voltage $v_{X\text{-}N}$ is a function of the diodes' state as determined by the three-phase voltage source $v_{SA\text{-}N}$, $v_{SB\text{-}N}$, $v_{SC\text{-}N}$, and the state variables $i_{X\text{-}N}$ and $v_{CO\text{-}N}$. If $i_{X\text{-}N} > 0$ or the largest positive line-to-line voltage is greater than $v_{CO\text{-}N}$, then the pair of diodes associated with the largest positive line-to-line voltage is on with $v_{X\text{-}N}$ equal to this line-to-line voltage, and $i_{X\text{-}N}$ circulates through the two line-to-neutral voltage sources associated with this line-to-line voltage. The current through the third line-to-neutral voltage source is zero. If $i_{X\text{-}N} = 0$ and the absolute value of the largest line-to-line voltage is less than $v_{CO\text{-}N}$, then all diodes are off, $v_{X\text{-}N} = v_{CO\text{-}N}$, and the currents through all voltage sources are zero.

The two state equations (2) and (3) are coded as a pair of Fortran subroutines, and a publicly available variable-time-step Runge–Kutta program [4] numerically integrates the state equations with respect to time to find the circuit waveforms in the periodic steady-state condition (PSSC). A Newton–Raphson-based iterative method [5] is used to aid convergence to the PSSC. After the PSSC is reached, the simulation generates fixed-time-step discrete-time waveforms in the PSSC over one normalized period $T_{S\text{-}N}$ with $m = 1024$ points per period and integration time step $T_{S\text{-}N}/m$. The m discrete points of normalized time are

$$t_N(j) = \frac{j}{m} T_{S\text{-}N} \qquad (j = 0, 1, 2, \cdots, m-1). \quad (4)$$

For the single-phase rectifier, the discrete-time representation of source voltage $v_{S\text{-}N}(j)$, line current is $i_{S\text{-}N}(j)$, filter input voltage $v_{X\text{-}N}(j)$ inductor current $i_{X\text{-}N}(j)$, and capacitor voltage $v_{CO\text{-}N}(j)$ are saved in a file for further analysis. For the three-phase rectifier, the discrete-time A line current $i_{SA\text{-}N}(j)$, filter input voltage $v_{X\text{-}N}(j)$, inductor current $i_{X\text{-}N}(j)$, and capacitor voltage $v_{CO\text{-}N}(j)$ are saved in a file for further analysis. The analysis of these waveforms is described in the next section.

V. Definitions and Analysis

This section defines rectifier line-current harmonics and power factor, where IEEE Standard 519 definitions are used, if possible [6]. In addition, analysis of discrete-time representations of rectifier waveforms for harmonic content and power factor is described. The definitions and analysis are illustrated with respect to the single-phase rectifier shown in Fig. 2(a), but when taken on a per-phase basis are identical for the three-phase rectifier shown in Fig. 2(b). An example of time waveforms for the single-phase rectifier with finite filter inductance are illustrated in Fig. 4.

The single-phase rectifier is driven by a sinusoidal voltage source:

$$v_{S\text{-}N}(j) = \sqrt{2}\, V_{S\text{-}N} \sin(2\pi f_{S\text{-}N} t_N(j)) \quad (5)$$

The rectifier current $i_{S\text{-}N}(j)$ is nonsinusoidal and periodic and is represented by the Fourier series:

$$\begin{aligned} i_{S\text{-}N}(j) &= i_{S(1)\text{-}N}(j) + \sum_{h>1} i_{S(h)\text{-}N}(j) \\ &= \sqrt{2} I_{S(1)\text{-}N} \sin(2\pi f_{S\text{-}N} t_N(j) + \phi_{S(1)}) \\ &\quad + \sqrt{2} \sum_{h>1} I_{S(h)\text{-}N} \sin[h(2\pi f_{S\text{-}N} t_N(j) + \phi_{S(h)})] \end{aligned} \quad (6)$$

and is composed of a fundamental $i_{S(1)\text{-}N}(j)$ and higher order harmonics $i_{S(h)\text{-}N}(j)$ where $h > 1$. The positive-going zero crossing of the source voltage at $t_N(j) = 0$ is the phase reference for the Fourier representation in (6), and the phase angles $\phi_{S(h)}$ of harmonic h in (6) are referenced to the fundamental (rather than the harmonic). A discrete Fourier transform (DFT) is used to find the rms value $I_{S(1)\text{-}N}$ and phase angle $\phi_{S(1)}$ of the fundamental as illustrated in Fig. 4, and the rms values $I_{S(h)\text{-}N}$ and phase angles $\phi_{S(h)}$ of the harmonics of $i_{S\text{-}N}(j)$.

The rms value $I_{S\text{-}N}$ of $i_{S\text{-}N}(j)$ is the square root of the sum of the squares of the fundamental and the harmonics:

$$I_{S\text{-}N} = \sqrt{I_{S(1)\text{-}N}^2 + \sum_{h>1} [I_{S(h)\text{-}N}]^2}. \quad (7)$$

Therefore, the rectifier current harmonics increase the rms value of the rectifier current above that of the fundamental alone. As a check, the rms value $I_{S\text{-}N}$ is found by taking the square root of the mean value of the squares of the m discrete values of $i_{S\text{-}N}(j)$ over one period:

$$I_{S\text{-}N} = \sqrt{\frac{1}{m} \sum_{j=0}^{m-1} i_{S\text{-}N}(j)^2}. \quad (8)$$

The real power $P_{S\text{-}N}$ supplied by the source is obtained

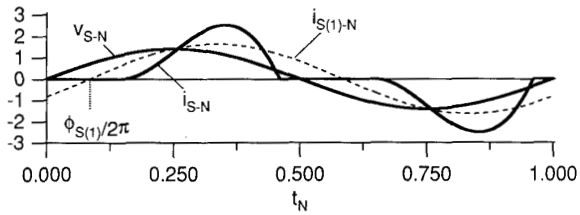

Fig. 4. Example of nonsinusoidal rectifier line current $i_{S\text{-}N}$ drawn from a sinusoidal source $v_{S\text{-}N}$ for finite output filter inductor. The line-current fundamental $i_{S(1)\text{-}N}$ lags the source voltage by angle $\phi_{S(1)}$.

$v_{S\text{-}N}(j) \cdot i_{S\text{-}N}(j)$ over one period:

$$P_{S\text{-}N} = \frac{1}{m} \sum_{j=0}^{m-1} v_{S\text{-}N}(j) i_{S\text{-}N}(j). \tag{9}$$

The circuit is lossless, and $P_{S\text{-}N}$, as calculated from simulation waveforms, is checked by comparison with the constant output power $P_{O\text{-}N}$. Since the source voltage $v_{S\text{-}N}(j)$ is a fundamental-frequency sinusoid, only the rectifier current fundamental $i_{S(1)\text{-}N}(j)$ contributes to real power $P_{S\text{-}N}$, and (9) reduces to

$$P_{S\text{-}N} = V_{S\text{-}N} I_{S(1)\text{-}N} \cos \phi_{S(1)}. \tag{10}$$

The rectifier power factor PF_S is the ratio of the real power $P_{S\text{-}N}$ to the apparent power $V_{S\text{-}N} \cdot I_{S\text{-}N}$ delivered by the source:

$$\mathrm{PF}_S = \frac{P_{S\text{-}N}}{V_{S\text{-}N} I_{S\text{-}N}} \tag{11}$$

$$\mathrm{PF}_S = \frac{V_{S\text{-}N} I_{S(1)\text{-}N} \cos \phi_{S(1)}}{V_{S\text{-}N} I_{S\text{-}N}} = \cos \phi_{S(1)} \frac{I_{S(1)\text{-}N}}{I_{S\text{-}N}}. \tag{12}$$

As a check, the rectifier power factor is calculated using both (11) and (12).

The expression for rectifier power factor (12) contains the familiar displacement power factor term $\cos \phi_{S(1)}$, in which $\phi_{S(1)}$ is the angle between the sinusoidal source voltage $v_{S\text{-}N}(j)$ and the sinusoidal rectifier current fundamental $i_{S(1)\text{-}N}(j)$. The displacement power factor is made unity by reduction of $\phi_{S(1)}$ to zero. In addition, the expression for rectifier power factor contains the term $I_{S(1)\text{-}N}/I_{S\text{-}N}$, which embodies the effects of rectifier line current harmonics on the overall power factor. The authors have been unable to find a generally accepted name for this term and have called it the "purity factor" (despite the moral overtones) because $I_{S(1)\text{-}N}/I_{S\text{-}N} = 1$ implies that $i_{S\text{-}N}(j)$ is a pure sinusoid with no harmonic content, whereas $I_{S(1)\text{-}N}/I_{S\text{-}N} < 1$ implies that $i_{S\text{-}N}(j)$ is a less-pure sinusoid with greater harmonic content. The purity factor is easily related to the familiar total harmonic distortion (THD) expressed in percent by

$$\mathrm{THD} = 100 \frac{\sqrt{\sum_{h>1} [I_{S(h)\text{-}N}]^2}}{I_{S(1)\text{-}N}} = 100 \sqrt{\frac{1}{(I_{S(1)\text{-}N}/I_{S\text{-}N})^2} - 1}. \tag{13}$$

Examination of (12) shows that a near-unity power factor rectifier must simultaneously have *both* a near-unity displacement power factor *and* a near-unity purity factor (or near-zero THD). In the remainder of the paper, the explicit dependence of the discrete-time circuit waveforms on (j) is omitted, for example, $v_{S\text{-}N}(j)$ is written as $v_{S\text{-}N}$, etc.

VI. Derivation of Design Relationships

The analysis by simulation determines the rectifier line-current fundamental and harmonics, displacement power factor, purity factor, and overall power factor for one combination of $V_{S\text{-}N}$ or $V_{SA\text{-}N} = V_{SB\text{-}N} = V_{SC\text{-}N}$, $f_{S\text{-}N}$, $L_{O\text{-}N}$, $C_{O\text{-}N}$, and $P_{O\text{-}N}$. Design relationships for line-current fundamental and harmonics, displacement power factor, purity factor, and overall power factor as a function of $L_{O\text{-}N}$ are derived by holding $V_{S\text{-}N}$ or $V_{SA\text{-}N} = V_{SB\text{-}N} = V_{SC\text{-}N}$, $f_{S\text{-}N}$, $C_{O\text{-}N}$, and $P_{O\text{-}N}$, constant and analyzing rectifier operation in the PSSC for discrete values of $L_{O\text{-}N}$ spaced at regular intervals.

The rectifier is simulated using nominal source voltage with $V_{S\text{-}N} = 1$ or $V_{SA\text{-}N} = V_{SB\text{-}N} = V_{SC\text{-}N} = 1$, nominal source frequency with $f_{S\text{-}N} = 1$, and with nominal output power so that $P_{O\text{-}N} = 1$. A conveniently large value of $C_{O\text{-}N} = 1000$ is found to be sufficient to keep the peak-to-peak output voltage ripple less than 0.2% for all values of $L_{O\text{-}N}$. However, smaller $C_{O\text{-}N}$ values do not dramatically affect the results especially for larger $L_{O\text{-}N}$.

VII. Verification

The simulation's accuracy is verified by comparison to waveforms and partial power factor data available in the literature [7]–[12]. In addition, rectifiers were constructed in the laboratory, and waveforms acquired by a Tektronix 11401 digitizing oscilloscope were transferred to a Macintosh IIx computer over the IEEE-488 instrumentation bus using a National Instruments IEEE-488 card and Labview software. The fidelity of the simulated time waveforms to the laboratory time waveforms is excellent. The laboratory time waveforms were also analyzed for line-current fundamental and harmonics, displacement power factor, purity factor, and overall power factor as a function of $L_{O\text{-}N}$ using (6)–(12) and the DFT. The laboratory measurements compare extremely well with the simulated data, both of which are shown in the following two sections that provide design relationships for line-current harmonics and power factor as a function of $L_{O\text{-}N}$ for single- and three-phase rectifiers.

VIII. Single-Phase Rectifier Design Relationships

This section presents design relationships for the rms value and phase angle of rectifier line-current fundamental and harmonics, and for rectifier displacement power factor, purity factor, and overall power factor as a function of normalized output filter inductance $L_{O\text{-}N}$ for the single-phase rectifier shown in Fig. 2(a). Portions of this problem have been examined by previous investigators

[7]–[9], but minimum rectifier line-current harmonics and their effect on power factor have not been previously directly examined. The previous investigators also provide design relationships for $V_{O\text{-}N}$ as a function of $L_{O\text{-}N}$ that are not reproduced in this paper.

Representative normalized single-phase rectifier simulation time waveforms of source voltage $v_{S\text{-}N}$, rectifier current $i_{S\text{-}N}$, filter input voltage $v_{X\text{-}N}$, and output-filter-inductor current $i_{X\text{-}N}$ are shown in Fig. 5 for three values of normalized output filter inductance. The conduction time intervals for each diode are also indicated. The time waveforms measured in the laboratory are essentially identical to the waveforms shown in Fig. 5. The waveforms of $i_{X\text{-}N}$ and $i_{S\text{-}N}$ are dramatically different for different output filter inductances, and Fig. 5 illustrates three distinct modes of operation which, adopting the nomenclature of Dewan [8], are the discontinuous conduction mode I (DCM I), discontinuous conduction mode II (DCM II), and continuous conduction mode (CCM), respectively.

The DCM I occurs for $L_{O\text{-}N} < 0.027$ and is illustrated in Fig. 5(a) for $L_{O\text{-}N} = 0.010$. The $i_{S\text{-}N}$ and $i_{X\text{-}N}$ waveforms are characterized by two short-duration high-peak-value current pulses during which either D_1 and D_4 conduct or D_2 and D_3 conduct. Two zero-current intervals separate the *single D_1 and D_4 conduction interval* and the *single D_2 and D_3 conduction interval.* The DCM II occurs for $0.027 < L_{O\text{-}N} < 0.043$ and is illustrated in Fig. 5(b) for $L_{O\text{-}N} = 0.037$. The DCM II is characterized by a zero-current interval separating *two D_1 and D_4 conduction intervals* and commutation from D_1 and D_4 to D_2 and D_3 at $t_N = 0.5$, and a zero-current interval separating *two D_2 and D_3 conduction intervals* with commutation from D_2 and D_3 to D_1 and D_4 at $t_N = 1.0$. The CCM occurs for $L_{O\text{-}N} > 0.043$ and is illustrated in Fig. 5(c) for $L_{O\text{-}N} = 0.090$. Diode conduction alternates at $t_N = 0.5$ and at $t_N = 1.0$ between a single D_1 and D_4 conduction interval and a single D_2 and D_3 conduction interval. As the name implies, *no zero-current interval* exists in the CCM. Comparison of Fig. 5(a), (b), and (c) shows the wide variation in rectifier-current waveforms that result from differing values of $L_{O\text{-}N}$, and comparison to Fig. 3(a) shows the severe error that is incurred by using a near-infinite-inductance approximation to represent finite $L_{O\text{-}N}$.

Figs. 6 and 7 show design relationships for single-phase rectifier line-current harmonics and power factor as obtained from both simulation and laboratory measurement. The simulation data are shown as continuous curves and the laboratory data are shown as discrete points. Fig. 6(a) shows the rms values—$I_{S(1)\text{-}N}$, $I_{S(3)\text{-}N}$, $I_{S(5)\text{-}N}$, $I_{S(7)\text{-}N}$, and $I_{S(9)\text{-}N}$—and Fig. 6(b) shows the phase angles—$\phi_{S(1)}$, $\phi_{S(3)}$, $\phi_{S(5)}$, $\phi_{S(7)}$, and $\phi_{S(9)}$—of the current fundamental, and the third, fifth, seventh, and ninth current harmonics, respectively, of the rectifier current $i_{S\text{-}N}$ as a function of $L_{O\text{-}N}$. As expected, all even-order harmonics are zero. Fig. 7 shows the relationship between the displacement power factor $\cos \phi_{S(1)}$, the purity factor $I_{S(1)\text{-}N}/I_{S\text{-}N}$, and the overall power factor PF_S as a function of $L_{O\text{-}N}$. The range of

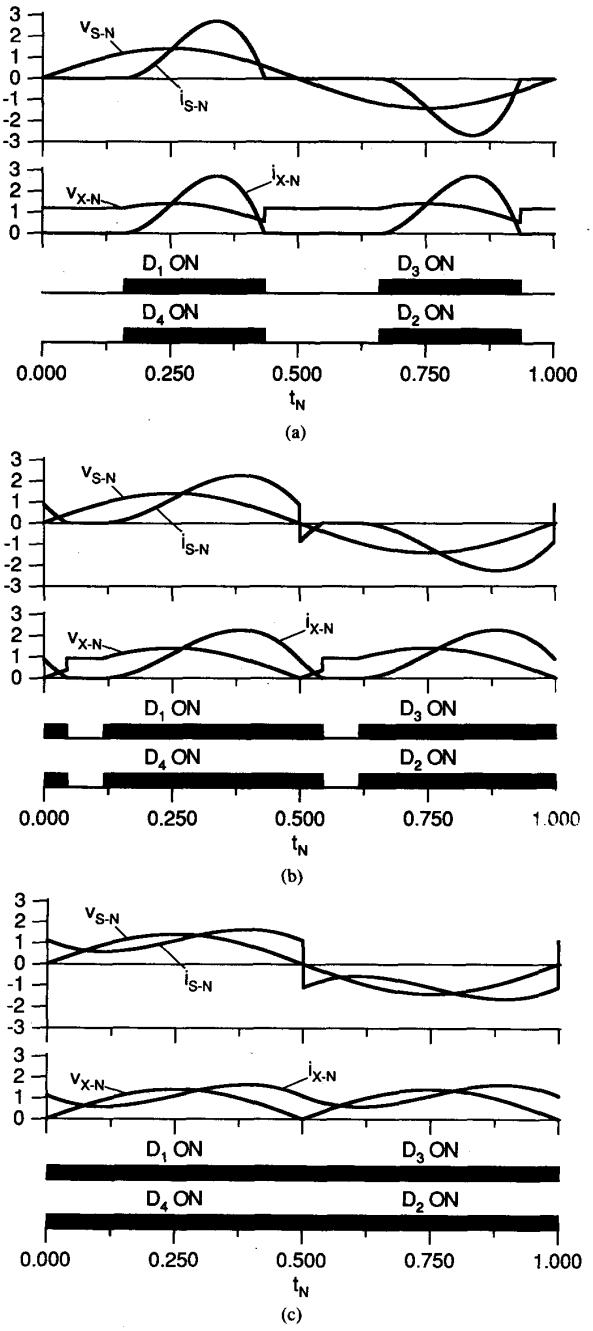

Fig. 5. Normalized single-phase rectifier waveforms: source voltage $v_{S\text{-}N}$, rectifier line current $i_{S\text{-}N}$, rectifier output voltage $v_{X\text{-}N}$, and output filter inductor current $i_{X\text{-}N}$ for (a) discontinuous conduction mode I (DCM I) for $L_{O\text{-}N} = 0.010$, (b) discontinuous conduction mode II (DCM II) for $L_{O\text{-}N} = 0.037$, and (c) continuous conduction mode (CCM) for $L_{O\text{-}N} = 0.090$. The conduction intervals for diodes D_1–D_4 are indicated by the shaded areas below the waveforms.

$L_{O\text{-}N}$ over which each conduction mode occurs is also indicated in Figs. 6 and 7. The laboratory measurements are nearly identical to the simulation confirming the accuracy of both. In addition, the design relationships for displace-

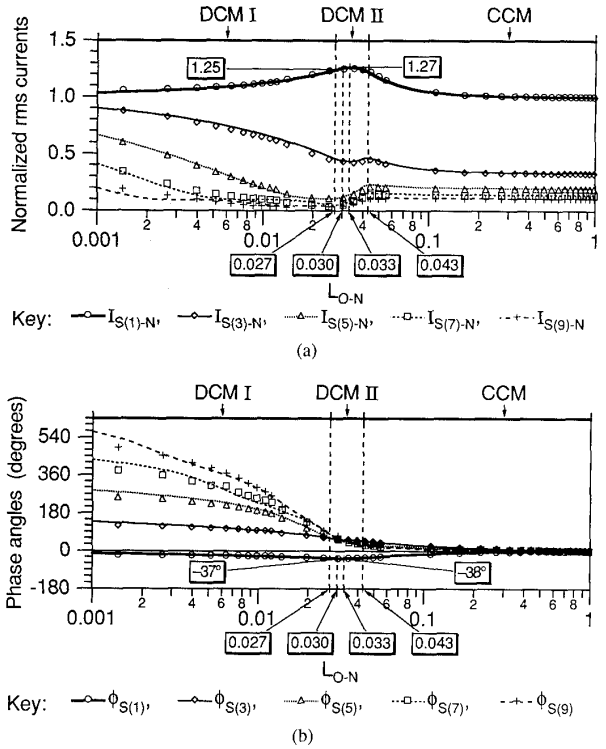

Fig. 6. Harmonics of single-phase rectifier line current $i_{S\text{-}N}$. (a) The normalized rms value $I_{S(1)\text{-}N}$ of the fundamental, and the normalized rms values $I_{S(3)\text{-}N}$, $I_{S(5)\text{-}N}$, $I_{S(7)\text{-}N}$, and $I_{S(9)\text{-}N}$ of the harmonics. (b) The phase angle $\phi_{S(1)}$ of the fundamental, and the phase angles $\phi_{S(3)}$, $\phi_{S(5)}$, $\phi_{S(7)}$, and $\phi_{S(9)}$ of the harmonics with respect to the source voltage $v_{S\text{-}N}$ as a function of normalized output filter inductance $L_{O\text{-}N}$. Simulation data are shown as continuous curves, and laboratory data are shown as discrete points.

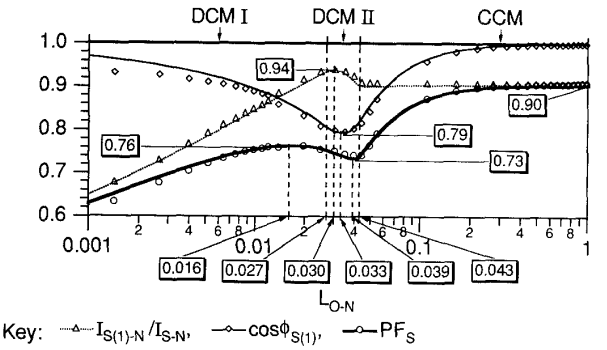

Fig. 7. Single-phase rectifier displacement power factor cos $\phi_{S(1)}$, purity factor $I_{S(1)\text{-}N}/I_{S\text{-}N}$, and overall power factor PF_S as a function of output filter inductance $L_{O\text{-}N}$. Simulation data are shown as continuous curves, and laboratory data are shown as discrete points.

ment power factor and overall power factor appear in the previously cited literature and match those shown in Fig. 7.

As shown in Fig. 6(b), the line-current fundamental phase angle $\phi_{S(1)}$ is near zero for small $L_{O\text{-}N}$, rises to the largest-magnitude phase angle $|\phi_{S(1)}| = 38°$ for $L_{O\text{-}N} = 0.033$, and returns to near zero for large $L_{O\text{-}N}$. Therefore, as shown in Fig. 7, the displacement power factor cos $\phi_{S(1)}$ is near unity for small $L_{O\text{-}N}$, falls to 0.79 for $L_{O\text{-}N} = 0.033$ and rises again to near unity for large $L_{O\text{-}N}$. Examination of (10) shows that since $V_{S\text{-}N}$ and $P_{O\text{-}N} = P_{S\text{-}N}$ are constant, the rms value of $I_{S(1)\text{-}N}$ of current fundamental as shown in Fig. 6(a) is inversely proprotional to cos $\phi_{S(1)}$.

As seen in Fig. 6(a), the normalized rms values $I_{S(h)\text{-}N}$ of the current harmonics are large for small $L_{O\text{-}N}$, are at a minimum for $L_{O\text{-}N}$ slightly less than that required to enter DCM II, slightly larger for $L_{O\text{-}N}$ in the DCM II range, and approach their near-infinite-inductance values in the CCM range. Therefore, in Fig. 7, the purity factor is low for small $L_{O\text{-}N}$, at a maximum of 0.94 for $L_{O\text{-}N} = 0.030$, and slightly lower at 0.90 for large $L_{O\text{-}N}$.

As shown by (12), the overall power factor PF_S is the product of the purity factor $I_{S(1)\text{-}N}/I_{S\text{-}N}$ and the displacement power factor cos $\phi_{S(1)}$, and, as shown in Fig. 7, these two influences are in conflict. For small $L_{O\text{-}N}$, the overall power factor is at a global minimum, despite the near-unity displacement power factor, because the rectifier current is very distorted and the purity factor is low. The overall power factor is at a local maximum $PF_S = 0.76$ for $L_{O\text{-}N} = 0.016$ because of the reduction in waveform distortion and the increase of purity factor. However, the overall power factor is at a local minimum $PF_S = 0.73$ for $L_{O\text{-}N} = 0.039$ because of the worsening displacement power factor. The overall power factor is at a global maximum $PF_S = 0.90$ for a near-infinite $L_{O\text{-}N}$ due to the improvement of displacement power factor and the relatively good purity factor.

The maximum overall $PF_S = 0.90$ occurs for near-infinite $L_{O\text{-}N}$. However, operation in this condition requires an uneconomically large and impractical output filter inductor. As noted by Dewan [8], maximum practical $PF_S = 0.76$ for a reasonably-sized output filter inductor occurs in DCM I with $L_{O\text{-}N} = 0.016$. The waveforms used in Fig. 4 to illustrate power factor are obtained in this operating condition. The minimum overall line-current harmonics occur not for near-infinite $L_{O\text{-}N}$ but for $L_{O\text{-}N} = 0.030$ where $I_{S(1)\text{-}N}/I_{S\text{-}N} = 0.94$.

As a design example, a $P_{O(\text{nom})} = 1200$ W, $V_{S(\text{nom})} = 120$ V, $f_{S(\text{nom})} = 60$ Hz rectifier has normalization references $V_{\text{REF}} = 120$ V, $P_{\text{REF}} = 1200$ W, $f_{\text{REF}} = 60$ Hz, $I_{\text{REF}} = 10$ A, and $Z_{\text{REF}} = 12\ \Omega$. Substitution of the normalization references and $L_{O\text{-}N} = 0.016$ into design equation (D.12) gives $L_O = 3.2$ mH for a maximum power factor design. Substitution of the normalization references and $L_{O\text{-}N} = 0.030$ into design equation (D.12) gives $L_O = 6$ mH a for minimum line-current harmonics design.

IX. Three-Phase Rectifier Design Relationships

This section presents design relationships for the rms value and phase angle of rectifier line-current fundamental and harmonics, and for rectifier displacement power factor, purity factor, and overall power factor as a function of normalized output filter inductance $L_{O\text{-}N}$ for the

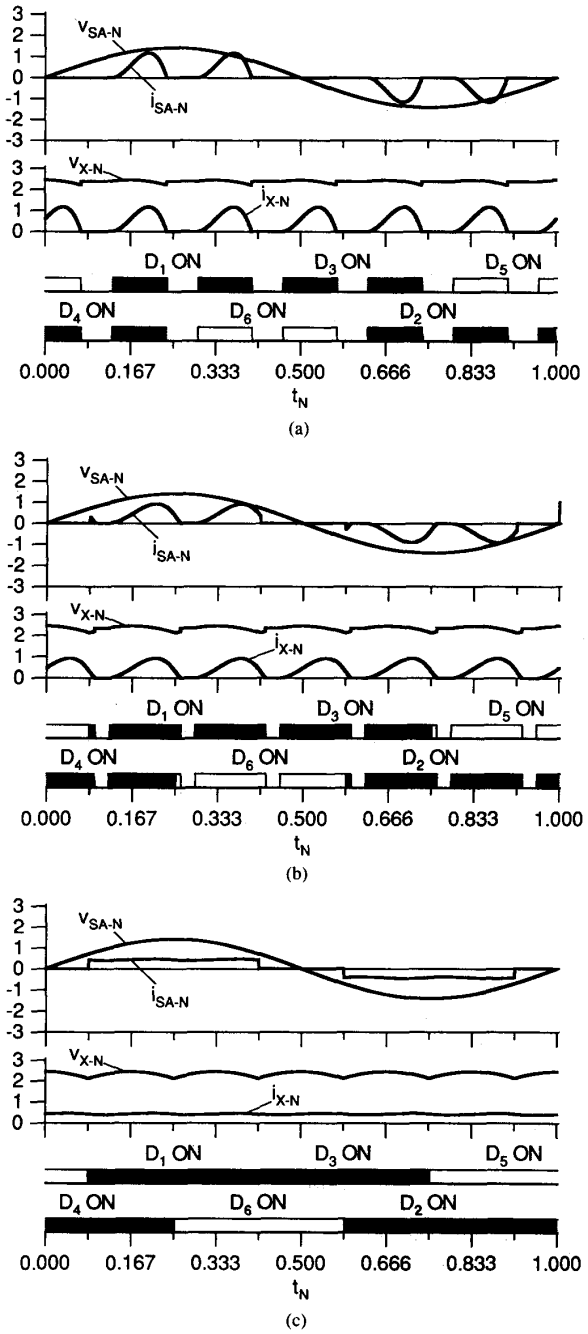

Fig. 8. Normalized three-phase rectifier waveforms: phase-A source voltage v_{SA-N}, phase-A rectifier line current i_{SA-N}, rectifier output voltage v_{X-N}, and output filter inductor current i_{X-N} for (a) discontinuous conduction mode I (DCM I) for $L_{O-N} = 0.0024$, (b) discontinuous conduction mode II (DCM II) for $L_{O-N} = 0.0064$, and (c) continuous conduction mode (CCM) for $L_{O-N} = 0.10$. The conduction intervals for diodes D_1–D_6 are indicated by the shaded areas below the waveforms.

three-phase rectifier shown in Fig. 2(b). Aspects of this problem have been treated by previous investigators [10]–[12], and the three-phase design relationships are presented for completeness, unification, and verification of prior work and for contrast with the single-phase rectifier. As with the single-phase rectifier, the previous investigators also provide three-phase rectifier design relationships for V_{O-N} as a function of L_{O-N} that are not reproduced in this paper.

Representative normalized three-phase rectifier time waveforms of phase-A source voltage v_{SA-N}, phase-A rectifier current i_{SA-N}, filter input voltage v_{X-N}, and output-filter-inductor current i_{X-N} are shown in Fig. 8 for three values of normalized output filter inductance. The conduction time interval for each diode is also indicated. The time waveforms measured in the laboratory are essentially identical to the waveforms shown in Fig. 8. The waveforms for phases B and C are produced by shifting the waveforms for phase A by one-third period and two-thirds period, respectively. The three-phase rectifier also exhibits DCM I, DCM II, and CCM operation, as illustrated in Fig. 8. As with the single-phase rectifier, a comparison of Fig. 8 with Fig. 3(b) reveals the significant error that results from assuming a finite L_{O-N} to be near-infinite. The description of the three modes of operation in the previous section for the single-phase rectifier is applicable to the three-phase rectifier, with the exception that three-phase rectifier has six diodes and six conduction intervals as opposed to the four diodes and two conduction intervals for the single-phase rectifier. The boundary between DCM I and II occurs for $L_{O-N} = 0.0050$, and the boundary between DCM II and CCM occurs for $L_{O-N} = 0.0083$.

Figs. 9 and 10 show design relationships for three-phase rectifier line-current harmonics and power factor as obtained from both simulation and laboratory measurement. The simulation data are shown as continuous curves and the laboratory data are shown as discrete points. Fig. 9(a) shows the rms values—$I_{SA(1)-N}$, $I_{SA(5)-N}$, $I_{SA(7)-N}$, $I_{SA(11)-N}$, and $I_{SA(13)-N}$—and Fig. 9(b) shows the phase angles—$\phi_{SA(1)}$, $\phi_{SA(5)}$, $\phi_{SA(7)}$, $\phi_{SA(11)}$, and $\phi_{SA(13)}$—of the current fundamental, and the fifth, seventh, eleventh, and thirteenth current harmonics, respectively, of the phase-A rectifier line current i_{SA-N} as a function of L_{O-N}. As expected, all even-order harmonics and all harmonics that are a multiple of three are zero. Fig. 10 shows the relationship between the displacement power factor cos $\phi_{SA(1)}$, the purity factor $I_{SA(1)-N}/I_{SA-N}$, and the overall power factor PF_{SA} as a function of L_{O-N}. The range of L_{O-N} over which each conduction mode occurs is also indicated in Figs. 9 and 10. The laboratory measurements are nearly identical to the simulation confirming the accuracy of both.

In contrast to the single-phase rectifier, the line-current fundamental phase angle $\phi_{SA(1)}$ as shown in Fig. 9(b) is near zero regardless of the value of L_{O-N}. The largest-magnitude phase angle $|\phi_{SA(1)}| = 12°$ and the minimum displacement power factor cos $\phi_{SA(1)} = 0.98$ occur for $L_{O-N} = 0.0055$ as shown in Figs. 9(b) and 10, respectively. Since the displacement power factor cos $\phi_{SA(1)} \approx 1$ regardless of L_{O-N}, $I_{SA(1)-N} \approx 0.33$ because one third of P_{O-N} is delivered by phase A and the remaining two thirds of P_{O-N} is delivered equally by phases B and C. Therefore,

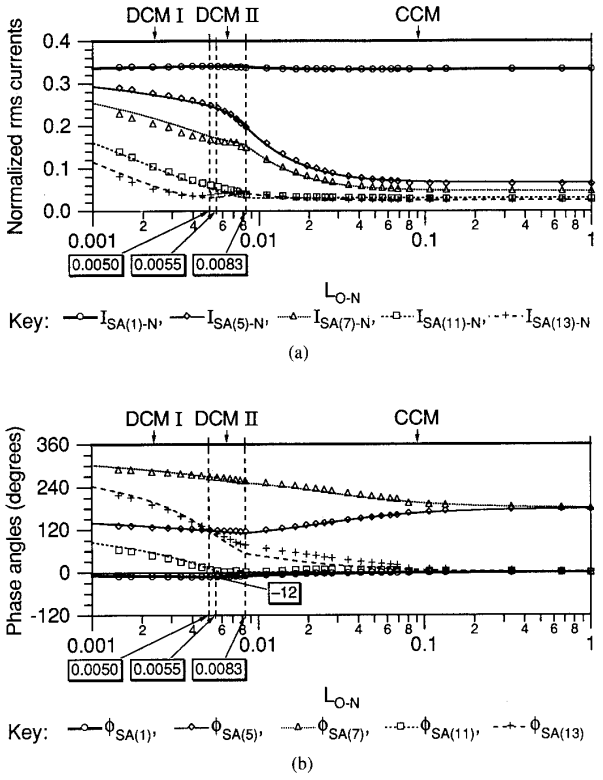

Fig. 9. Harmonics of three-phase rectifier phase-A line current $i_{SA\text{-}N}$. (a) Normalized rms value $I_{SA(1)\text{-}N}$ of the fundamental, and the normalized rms values $I_{SA(5)\text{-}N}$, $I_{SA(7)\text{-}N}$, $I_{SA(11)\text{-}N}$, and $I_{SA(13)\text{-}N}$ of the harmonics. (b) The phase angle $\phi_{SA(1)}$ of the fundamental, and phase angles $\phi_{SA(5)}$, $\phi_{SA(7)}$, $\phi_{SA(11)}$, and $\phi_{SA(13)}$ of the harmonics with respect to the line-to-neutral voltage $v_{SA\text{-}N}$ as a function of normalized output filter inductance $L_{O\text{-}N}$. Simulation data are shown as continuous curves, and laboratory data are shown as discrete points.

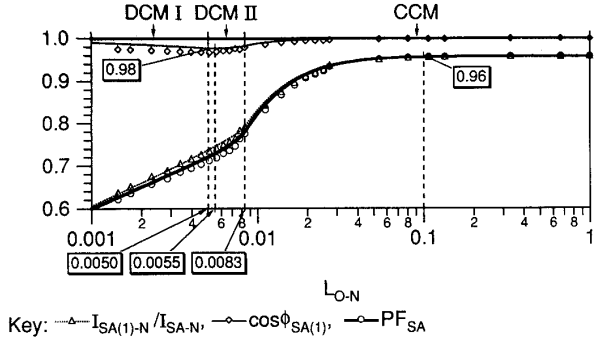

Fig. 10. Three-phase rectifier displacement power factor cos $\phi_{SA(1)}$, purity factor $I_{SA(1)\text{-}N}/I_{SA\text{-}N}$, and overall power factor PF_{SA} of phase-A as a function of output filter inductance $L_{O\text{-}N}$. Simulation data are shown as continuous curves, and laboratory data are shown as discrete points.

$L_{O\text{-}N}$ has almost no influence on displacement power factor, and the rectifier line-current harmonics and the purity factor are the dominant influences on the overall power factor.

As shown by Fig. 9(a), the line-current harmonics are high for small $L_{O\text{-}N}$ values and, except for a small portion of $I_{SA(13)\text{-}N}$, decrease uniformly for larger $L_{O\text{-}N}$ values, reaching a minimum at $L_{O\text{-}N} \approx 0.10$. Therefore, the purity factor $I_{SA(1)\text{-}N}/I_{SA\text{-}N}$ and the overall power factor PF_{SA} are low for small $L_{O\text{-}N}$ values and incrase to a maximum $I_{SA(1)\text{-}N}/I_{SA\text{-}N} = PF_{SA} = 0.96$ for $L_{O\text{-}N} = 0.10$. A larger value of $L_{O\text{-}N}$ does not significantly improve displacement power factor or overall power factor. Therefore, $L_{O\text{-}N} = 0.10$ is a reasonable approximation to a near-infinite output-filter inductance.

Consider a modification of the previous design example in which $P_{O(\text{nom})} = 1200$ W, $V_{SA(\text{nom})} = V_{SB(\text{nom})} = V_{SC(\text{nom})} = 120$ V line-to-neutral, and $f_{S(\text{nom})} = 60$ Hz. The normalization references are $V_{\text{REF}} = 120$ V, $P_{\text{REF}} = 1200$ W, $f_{\text{REF}} = 60$ Hz, $I_{\text{REF}} = 10$ A, and $Z_{\text{REF}} = 12\ \Omega$. Substitution of the normalization references and $L_{O\text{-}N} = 0.10$ into design equation (D.12) gives $L_O = 20$ mH.

A designer might be tempted to conclude that the single-phase rectifier requires a physically smaller inductor by comparing $L_O = 20$ mH for a maximum-power-factor three-phase rectifier to $L_O = 3.2$ mH for a maximum-power-factor single-phase rectifier. However, comparison of Figs. 5 and 8 shows a substantially higher $v_{X\text{-}N}$, and a substantially lower $i_{X\text{-}N}$ for the three-phase rectifier as compared to the single-phase rectifier for the same normalized output power $P_{O\text{-}N} = 1$. Since inductor physical size depends both on inductance value and inductor current, conclusions based on inductance value alone are misleading.

X. Summary

Classical rectifier analysis based on near-infinite output filter inductance and near-constant filter inductor current becomes less satisfactory as line-current harmonics and power factor issues increasingly concern power-systems and power-electronics engineers. This paper provides quantitative design data for line-current harmonics and power factor for single and three-phase rectifiers for realistic design situations with finite output-filter inductance and appreciable current ripple. These data provide a reference for designers of new equipment and for the evaluation of harmonic and power factor problems caused by existing equipment.

The maximum power factor for a single-phase rectifier using an infinite output filter inductor is 0.90, but the maximum power factor for a reasonably-sized finite-inductance rectifier is 0.76. However, this operating condition does not result in minimum rectifier line-current harmonics. Design of the rectifier for minimum line-current harmonics produces a purity factor of 0.94. The maximum power factor for a three-phase rectifier is 0.96 and occurs for an infinite output inductance. This operating condition also results in minimum line-current harmonics. Power factor is not significantly improved, nor are line-current harmonics significantly reduced for output filter inductances larger than a crucial value.

ACKNOWLEDGMENT

The authors thank L. Hall and E. Reese for their assistance in assembling the instrumentation and conducting line-current harmonics and power factor measurements.

REFERENCES

[1] J. Schaefer, *Rectifier Circuits, Theory and Design.* New York: Wiley, 1965.

[2] A. W. Kelley, T. G. Wilson, and H. A. Owen, Jr., "Analysis of the two-coil model of the ferroresonant transformer with a rectified output in the low-line heavy-load minimum-frequency condition," *1983 International Telecommunications Energy Conf. Rec.* (INTELEC '83), Tokyo, Japan, October 1983, pp. 374–381.

[3] E. B. Sharodi and S. B. Dewan, "Simulation of the six-pulse bridge converter with input filter," *1985 Power Electronics Specialists' Conf. Rec.* (PESC'85), Toulouse, France, June 1985, pp. 502–508.

[4] G. E. Forsythe, M. A. Malcolm, and C. B. Moler, *Computer Methods for Mathematical Computations.* Englewood Cliffs, NJ: Prentice-Hall, 1977, ch. 6.

[5] F. R. Colon and T. N. Trick, "Fast periodic steady-state analysis for large-signal electronic circuits," *IEEE J. Solid-State Circuits*, vol. SC-8, no. 4, pp. 260–269, Aug. 1973.

[6] "IEEE guide for harmonic control and reactive compensation of static power converters," IEEE/ANSI Standard 519, 1981.

[7] F. C. Schwarz, "Time-domain analysis of the power factor for a rectifier-filter system with over- and subcritical inductance," *IEEE Trans. Ind. Electron. Contr. Instrum.*, vol. IECI-20, no. 2, pp. 61–68, May 1973.

[8] S. B. Dewan, "Optimum input and output filters for single-phase rectifier power supply," *IEEE Trans. Industry Applications*, vol. IA-17, no. 3, pp. 282–288, May/June 1981.

[9] California Institute of Technology, Power Electronics Group, "Input-current shaped ac-to-dc converters, final report," NASA-CR-176787, prepared for NASA Lewis Research Center, pp. 1–49, May 1986.

[10] M. Grötzbach, B. Draxler, and J. Schörner, "Line harmonics of controlled six-pulse bridge converters with dc ripple," *Rec. 1987 IEEE Industry Applications Society Annu. Meet.*, part I, Atlanta, GA:, Oct. 1987, pp. 941–945.

[11] S. W. H. De Haan, "Analysis of the effect of source voltage fluctuations of the power factor in three-phase controlled rectifiers," *IEEE Trans. Industry Applications*, vol. IA-22, no. 2, pp. 259–266, March/April 1986.

[12] M. Sakui, H. Fujita, and M. Shioya, "A method for calculating harmonic currents of a three-phase bridge uncontrolled rectifier with dc filter," *IEEE Trans. Ind. Electron.*, vol. IE-36, no. 3, pp. 434–440, Aug. 1989.

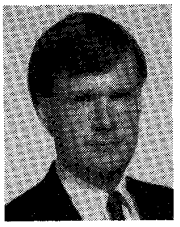

Arthur W. Kelley (S'78, M'85) was born in 1957 in Norfolk, VA. He received the B.S.E. degree from Duke University, Durham, NC, in 1979. He continued at Duke as a James B. Duke Fellow and received the M.S., and Ph.D. degrees in 1981, and 1984, respectively.

From 1985 to 1987, Dr. Kelley was employed as a Senior Research Engineer at Sundstrand Corporation, Rockford, IL, where he worked on power electronics applications to aerospace power systems. He joined the faculty of the Department of Electrical and Computer Engineering at North Carolina State University in 1987 where he currently holds the rank of Assistant Professor. His interests in power electronics include PWM dc-to-dc converters, line-interfaced ac-to-dc converters and power quality, magnetic devices, magnetic materials, and computer-aided analysis and design of nonlinear circuits.

Dr. Kelley is a member of Sigma Xi, Phi Beta Kappa, Tau Beta Pi, and Eta Kappa Nu.

William F. Yadusky (S'87, M'90) received the B.A. degree in English from the University of North Carolina, Chapel Hill, in 1982, and the B.S.E.E. from North Carolina State University, Raleigh, in 1987. He was certified as an Engineer in Training in 1987.

Mr. Yadusky worked as a Graduate Research Assistant with the Electric Power Research Center at North Carolina State University under Dr. Arthur W. Kelley in 1988 and 1989. In 1990, Mr. Yadusky joined the Exide Electronics Technology Center, Raleigh, NC, where he helped develop selectable-input/selectable-output on-line uninterruptible power systems, PWM inverters, and printed cirucits. As an electrical design engineer on the Advanced Technology Development team, Mr. Yadusky is presently responsible for designing and developing high-voltage PWM rectifiers and high-frequency magnetic structures for uninterruptible power systems, frequency converters, and power conditioners.